

Improved crystallographic compatibility and magnetocaloric reversibility in Pt substituted $\text{Ni}_2\text{Mn}_{1.4}\text{In}_{0.6}$ magnetic shape memory Heusler alloy

K. K. Dubey¹, P. Devi^{2,3}, Anupam K. Singh¹ and Sanjay Singh^{1*}

¹School of Materials Science and Technology, Indian Institute of Technology (BHU), Varanasi-221005, India

²Max Planck Institute for Chemical Physics of Solids, Nothnitzer Str. 40, 01187 Dresden

³Ames Laboratory, US Department of Energy, Iowa State University, Ames, Iowa 50011, USA

Abstract

We present here the improved crystallographic/geometric compatibility and magnetocaloric reversibility by measurement of magnetic entropy change using different protocols in 10% Pt substituted $\text{Ni}_2\text{Mn}_{1.4}\text{In}_{0.6}$ magnetic shape memory alloy. The substitution of Pt reduces the thermal hysteresis about 50% to the $\text{Ni}_2\text{Mn}_{1.4}\text{In}_{0.6}$. The origin of the reduced thermal hysteresis is investigated by the crystallographic compatibility of the austenite and martensite phases. The calculated middle eigenvalue of the transformation matrix turned out to be 0.9982, which is very close to 1 (deviation is only 0.18%) suggests for the crystallographic compatibility between the austenite and martensite phases in $\text{Ni}_{1.9}\text{Pt}_{0.1}\text{Mn}_{1.4}\text{In}_{0.6}$. A very small thermal hysteresis and crystallographic compatibility between two phases in this alloy system indicate a stress-free transition layer (i.e. perfect habit plane) between the austenite and martensite phase, which is expected to give reversible martensite phase transition and therefore reversible magnetocaloric effect (MCE) as well. The calculated value of the isothermal entropy change (ΔS_{iso}) using the magnetization curve under three different measurement protocols (i.e. isothermal, loop, and isofield measurement protocol) is found to be nearly same indicating a reversible MCE in the present alloy system. Our work provides a path to design new magnetic shape memory Heusler

alloys for magnetic refrigeration and also suggest that any of the above measurement protocol can be used for the calculation of ΔS_{iso} for materials satisfying geometrical compatibility condition.

1. Introduction

A magnetic material heats up or cools down with the application of magnetic field in adiabatic condition and this phenomena is known as the magnetocaloric effect (MCE). MCE has created enormous interest in the solid state cooling technology [1-4] and typically presents in all the magnetic materials to some extent. The value of MCE is large near the first order magnetic phase transition (FOMT)/ first-order magnetostructural (martensite) phase transition (FOMST) where magnetization changes abruptly [5-7]. A giant MCE has been reported in various systems around their FOMT/FOMST phase transition e.g. in $Gd_5Si_2Ge_2$ [8], La-Fe-Si-based $(Fe, Si)_{13}$ [9, 10], Mn-As based [11], $Gd_5(Si_{1-x}Ge_x)_4$ [8] and magnetic shape memory Heusler alloys (e.g. $Ni_{2+x}Mn_{1-x}Z$; Z=Ga, In, Sn, and Sb) [5, 12-14]. Among these materials, magnetic shape memory Heusler alloys (MSMAs) have emerged as the suitable candidate for magnetic refrigeration applications due to their large MCE, rare earth free alloy design, no-toxic elements and their transition temperature can be easily tuned by varying composition [15, 16]. A large amount of work has been done on Ni-Mn based MSMAs aiming application as MCE material [5, 6, 12, 17-25]. The large MCE in MSMAs is mainly related to their FOMST. However, the same FOMST, which gives rise to the giant MCE, is also responsible for the irreversibility of the phase transition under the repeating magnetic field cycles and this became a major challenge in magnetic refrigeration devices [17, 21, 26-30]. This irreversibility is associated with the thermal hysteresis of FOMST due to a large stress at the transition layer between the austenite and the martensite phases. Therefore, more recently, the science community has given more focus on the minimization of the hysteresis [19, 21, 31-33]. Hysteresis is the intrinsic nature of the materials

undergoing FOMT/FOMST, and the one way to reduce hysteresis is by substituting the extra atom (few %) on a particular atomic site [7, 16]. Recently, a study on the structural and magnetic properties of Pt substituted Ni₂MnGa [7] is done, where it has been observed that the replacement of the Ni by Pt not only brings the martensite transition temperature close to the room temperature but also reduces the thermal hysteresis [7]. It has been proposed later that the Pt substitution might facilitate the requirement of the invariant habit plane [34], which supports shape memory behavior i.e. reversible martensite transition. This suggests that Ni-Pt-Mn-Ga are good candidate for magnetic actuators and magnetic cooling applications. Comparing the MCE of different Ni-Mn based MSMA it turns out that Ni₂Mn_{1.4}In_{0.6} is one of the best composition for the MCE application due to its large entropy and adiabatic temperature change although the irreversibility with repeating magnetic field cycle is a major challenge [6, 17, 21, 23, 30, 35-37]. Therefore, we selected this composition for our study and investigated the effect of 10% Pt substitution in Ni₂Mn_{1.4}In_{0.6} MSMA. Ni₂Mn_{1.4}In_{0.6} shows martensite transition near room temperature with a thermal hysteresis of ~8 K [38]. A 10% substitution of Pt in Ni₂Mn_{1.4}In_{0.6} reduces thermal hysteresis about 50% and the obtained MSMA composition i.e. Ni_{1.9}Pt_{0.1}Mn_{1.4}In_{0.6} exhibits a narrow thermal hysteresis ~4 K. We investigated the origin of the reduced hysteresis via calculation of the structural transformation matrix and crystallographic compatibility factor based on the lattice parameters obtained from the structural analysis of synchrotron X-ray powder diffraction (SXRPD) data in both austenite and martensite phases. The middle eigenvalue (λ_2) of the transformation matrix is found to be very close to 1 and smaller deviation from unity than the previously reported values in these alloys [21, 39, 40] suggests a low energy barrier or the stress free transition layer between austenite and martensite phases, which provides geometrical compatibility between two phases. Therefore, it is expected to show a reversible phase transition and MCE [40]. An indirect evidence

of reversibility is obtained from the calculation of magnetic entropy change using different measurement protocols as suggested in the literature [41]. The similar value of magnetic entropy change further indicates the reversibility of MCE.

2. Experimental

A polycrystalline ingot of $\text{Ni}_{1.9}\text{Pt}_{0.1}\text{Mn}_{1.4}\text{In}_{0.6}$ was prepared by arc melting in argon atmosphere [12, 23, 42]. The sample was melted four times for homogeneity and subsequently annealed in an evacuated sealed quartz ampoule at 900 °C for 24 h and then quenched in the ice water mixture. For the characterization, a part of the bulk sample was crushed into powder and then annealed under vacuum to remove residual stress-induced effects generated after crushing [43-45]. Magnetization measurement was performed by using magnetic property measurement system (Quantum Design) at a low magnetic field of 0.05 T in the temperature range 100 K to 375 K to determine the transition temperatures, range of transition and thermal hysteresis at the phase transition. To investigate the crystal structure and to determine the crystallographic compatibility condition, SXRPD data were recorded in both austenite and martensite phases using P02 beamline at Petra III, Hamburg, Germany by using a wavelength of 0.20712 Å. Further to calculate ΔS_{iso} , magnetization data were recorded using magnetic property measurement system (Quantum Design) in three measurement protocols named as isothermal, loop, and isofield protocol [46-50]. In isofield measurement protocol magnetization (M) vs temperature (T) data in the range of 150 K to 400 K were recorded during field cooled cooling (FCC) and field cooled warming (FCW) at different magnetic field values of 1 T, 3 T, 4 T, and 7 T. Magnetization vs field (H) data were recorded in isothermal and loop measurement protocols from the temperature range 210 K to 321 K at the step of 3 K up to 7 T applied field. For the simplicity of figure we show here $M(H)$ data

around martensite phase transition region (231 K to 273 K) at the step of 3 K up to 7 T applied field.

3. Results and discussion

The magnetization ($M(T)$) curves for the parent compound ($\text{Ni}_2\text{Mn}_{1.4}\text{In}_{0.6}$) and Pt doped compound, i.e. $\text{Ni}_{1.9}\text{Pt}_{0.1}\text{Mn}_{1.4}\text{In}_{0.6}$ under a low applied magnetic field of 0.05 T are shown in figure 1(a) and figure 1(b), respectively. The $M(T)$ curve for the parent compound (figure 1(a)) is obtained from Ref [38]. Both the alloys undergo magneto-structural (martensite) phase transition upon cooling (FCC curve) and reverse martensite transition during heating (FCW curve). The hysteresis observed during heating and cooling is the signature of the first-order phase transition. The characteristic temperatures related to the martensite phase transformations, i.e. martensite start (M_s), martensite finish (M_f), austenite start (A_s), and austenite finish temperature (A_f) for the $\text{Ni}_2\text{Mn}_{1.4}\text{In}_{0.6}$ are 296 K, 221 K, 232 K, and 301 K, respectively (figure 1(a)). For $\text{Ni}_{1.9}\text{Pt}_{0.1}\text{Mn}_{1.4}\text{In}_{0.6}$ these temperatures, i.e. M_s , M_f , A_s , and A_f are 281 K, 238 K, 243 K, and 284 K, respectively (figure 1(b)). The ferromagnetic transition temperature (T_C) for $\text{Ni}_2\text{Mn}_{1.4}\text{In}_{0.6}$ and $\text{Ni}_{1.9}\text{Pt}_{0.1}\text{Mn}_{1.4}\text{In}_{0.6}$ are ~ 314 K and ~ 304 K, respectively. The width of thermal hysteresis of the martensite transition is calculated from the martensite and austenite characteristic transition temperatures (M_s , M_f and A_s , A_f) using the formula $\frac{[(A_f+A_s)\sim(M_f+M_s)]}{2}$. The thermal hysteresis for the parent compound ($\text{Ni}_2\text{Mn}_{1.4}\text{In}_{0.6}$) is ~ 8 K, while hysteresis reduces to ~ 4 K for $\text{Ni}_{1.9}\text{Pt}_{0.1}\text{Mn}_{1.4}\text{In}_{0.6}$ (figure 1(b)). This value of thermal hysteresis is smaller in comparison to the other reported MSMA [21, 39, 41]. Recently a reversible MCE is reported in $\text{Ni}_{2.2}\text{MnGa}$ MSMA, where thermal hysteresis around martensite transition is observed about 5 K [41]. It has been suggested in the literature that the thermal hysteresis observed around the martensite transition is a direct consequence of the structural compatibility between austenite and martensite phases,

which is known as the crystallographic compatibility criteria [21, 39, 41, 51-56]. This crystallographic compatibility between austenite and martensite phases depends on the crystal structure/unit cell parameters of the austenite and martensite phases [55-58]. In order to investigate the crystal structure of the austenite and martensite phases and to get the actual unit cell parameters, temperature dependent SXRPD data were collected in both the austenite phase (350 K) and martensite phase (110 K). Le Bail refinements of SXRPD data of both the phases were done (figure 2 and figure 3) using Fullprof software package [59]. The austenite phase was refined by cubic $L2_1$ structure (space group $Fm-3m$) as expected in these alloys [23]. The refined lattice parameter turned out to be 6.0149 Å. Figure 2 shows that the observed and calculated peak profile are well matched, confirming the cubic structure of the austenite phase. The diffraction pattern of the martensite phase (figure 3) has large number of peaks indicating a modulated martensite phase as reported in the literature for Ni-Mn based MSMAAs [7, 42, 60]. It has been suggested that the low temperature structure of parent compound ($Ni_2Mn_{1.4}In_{0.6}$) is $3M$ modulated monoclinic with space group $I2/m$ [38]. A detailed investigation of martensite structure after 10% Pt doping in parent compound i.e. $Ni_{1.9}Pt_{0.1}Mn_{1.4}In_{0.6}$ was done using Le Bail refinements. Firstly, the structure of parent compound (i.e. $3M$ modulated monoclinic) was considered during the refinement but a clear mismatch between observed and calculated profiles was noticed as shown in figure 3(a). Some of the peaks were not indexed and they are indicated by arrows in the inset of figure 3(a). In the next step to identify these peaks, a larger unit cell i.e. $5M$ modulated unit cell was considered but this structure was also unable to identify all the Bragg peaks (shown in the inset of figure 3(b)). After trying many crystal structure combinations (not shown here), we found that all the Bragg reflections of the martensite phase at 110 K can be indexed by a monoclinic unit cell (space group $P2/m$) and lattice parameter $a=4.4172\text{Å}$, $b=5.6102\text{Å}$, $c=13.0350\text{Å}$, and $\beta=93.361^\circ$ (figure 3(c)).

Here, $c \sim 3 \cdot a$ indicating a $3M$ modulated monoclinic structure of the martensite phase [42, 60-62] of $\text{Ni}_{1.9}\text{Pt}_{0.1}\text{Mn}_{1.4}\text{In}_{0.6}$.

Having obtained the crystal structure and lattice parameters of the austenite and martensite phases of $\text{Ni}_{1.9}\text{Pt}_{0.1}\text{Mn}_{1.4}\text{In}_{0.6}$, now we turn the discussion towards the investigation of crystallographic compatibility criteria proposed for the reversible martensite transformation. It has been reported that the lattice parameter of the high symmetry austenite phase and low symmetry martensite phase are related by a transformation matrix U (equation (1)) [54, 55, 58, 63, 64], which is a 3×3 homogenous matrix defined as deformation matrix [21, 58, 65]. In the case of the complete reversibility of the martensite transformation, the λ_2 of the U should approach 1. The components of the transformation matrix depend entirely on the lattice parameters of the austenite (high temperature) and martensite (low temperature) phases, as described below [40, 41, 52, 53, 63, 65, 66].

$$U = \begin{bmatrix} \tau & \sigma & 0 \\ \sigma & \rho & 0 \\ 0 & 0 & \delta \end{bmatrix} \quad (1)$$

The components of the transformation matrix (τ , ρ , σ , and δ) are expressed as follows:

$$\tau = \frac{\alpha^2 + \gamma^2 + 2\alpha\gamma(\sin \beta - \cos \beta)}{2\sqrt{\alpha^2 + \gamma^2 + 2\alpha\gamma(\sin \beta)}} \quad (2)$$

$$\rho = \frac{\alpha^2 + \gamma^2 + 2\alpha\gamma(\sin \beta + \cos \beta)}{2\sqrt{\alpha^2 + \gamma^2 + 2\alpha\gamma(\sin \beta)}} \quad (3)$$

$$\sigma = \frac{\alpha^2 - \gamma^2}{2\sqrt{\alpha^2 + \gamma^2 + 2\alpha\gamma(\sin \beta)}} \quad (4)$$

$$\delta = \frac{b}{a_0} \quad (5)$$

where, $\alpha = \sqrt{2} \frac{a}{a_0}$, $\gamma = \sqrt{2} \frac{c}{Na_0}$, a_0 is the lattice parameter of the austenite (cubic) unit cell and a , b , c , and β denote the lattice parameter of the martensite (monoclinic) unit cell. N is the degree of modulation (in the present case $N=3$). Using the lattice parameters obtained from the Le Bail

refinements of the SXRPD data we calculated the components of the U for $Ni_{1.9}Pt_{0.1}Mn_{1.4}In_{0.6}$ and which turned out as:

$$U = \begin{bmatrix} 1.0598 & 0.0085 & 0 \\ 0.0085 & 0.9994 & 0 \\ 0 & 0 & 0.9327 \end{bmatrix}$$

The eigenvalues of the U are then calculated by simple mathematical calculations for a matrix. The eigen values turned out to be $\lambda_1=0.9327$, $\lambda_2=0.9982$, and $\lambda_3=1.0610$. Thus, the middle eigen value (λ_2) is 0.9982, which is nearly equal to 1 and its deviation from unity is only 0.0018 (i.e. 0.18%), which is smaller than previously reported value [21, 39, 40, 51]. Interestingly, the value of λ_2 is smaller than that of the parent compound $Ni_2Mn_{1.4}In_{0.6}$ as well for which the value of λ_2 is 1.0042 (calculated using lattice parameters reported in Ref [38]) and therefore its deviation from unity is 0.0042 (i.e. 0.42%). Thus the analysis of SXRPD data and U together explain the origin of reduced hysteresis after 10% Pt substitution in $Ni_2Mn_{1.4}In_{0.6}$. There are some recent reports on systems satisfying crystallographic compatibility condition (i.e. the value of λ_2 is very close to 1) and gives rise to a lower value of thermal hysteresis, which results into a reversible MCE [33, 67, 68]. These results clearly show that $Ni_{1.9}Pt_{0.1}Mn_{1.4}In_{0.6}$ has low thermal hysteresis and also crystallographic compatibility criteria has been improved. Therefore, in this alloys system, a field induced reversible martensite phase transition and hence, the reversible MCE is expected [33]. In general, there are two methods to estimate MCE. The first method is the “direct measurement method” where the adiabatic temperature change is measured directly under external applied magnetic field cycles [17, 21, 40, 41]. The second method is known as the “indirect measurement method” where ΔS_{iso} is measured using the magnetic hysteresis loop. For the indirect measurement of MCE different measurement protocols have been suggested for the calculation of the ΔS_{iso} especially for the FOMT/FOMST [20, 27, 48, 50, 69-75]. These measurement protocols are not only used to comment on the correct value of ΔS_{iso} but also useful to comment on the

reversibility/irreversibility of MCE [33, 49]. If these indirect measurement protocols provide a similar value of ΔS_{iso} then a reversible MCE is expected [46]. Therefore, now we proceed for the calculation of the ΔS_{iso} using magnetization measurement under three different protocols reported in the literature and named as isothermal, loop, and isofield protocol as discussed in the experimental section [46-48, 70, 76]. Following isothermal protocol, isothermal $M(H)$ curves are shown around the phase transition region between 231 K to 273 K with 3 K intervals (figure 4(a)). For loop measurement protocol the sample was heated up to 400 K to ensure the full austenite phase followed by cooling without application of the magnetic field down to 200 K to ensure the complete martensite phase transition and then subsequently sample was heated up to the desired measurement temperature where the $M(H)$ data were recorded (figure 4(b)) [41, 48, 70, 76]. Using these $M(H)$ curves, ΔS_{iso} is calculated using Maxwell's equation.

$$\Delta S_{iso} = \mu_0 \int_0^H \left(\frac{\partial M}{\partial T} \right)_H dH \quad (6)$$

For isofield measurement protocol, $M(T)$ during heating and cooling was recorded at different representative fields (1 T, 3 T, 4 T, and 7 T) as shown in the figure 4(c). For the ΔS_{iso} calculation, $M(H)$ data were extracted at different temperatures around the phase transition regions from these isofield curves manually. To take $M(H)$ data from the isofield curve, first the temperature was fixed, and the value of M and corresponding H from all isofield curves were noted down. This procedure provided the $M(H)$ curve at a fixed temperature. Similarly, $M(H)$ data is extracted for all other temperatures, which provided a series of the $M(H)$ curves at different temperatures (figure 4(d)). Then using Maxwell's relation (equation (6)) ΔS_{iso} was calculated for different field values similar to the other two (isothermal and loop) measurement protocols. The calculated value of ΔS_{iso} as a function of temperature is compared for all three measurement protocols at field values of 1 T, 3 T, 4 T, and 7 T (figure 5). It is interesting to note

that the values of the ΔS_{iso} at different fields are unambiguously the same for all three measurement protocols suggesting a reversible MCE in $Ni_{1.9}Pt_{0.1}Mn_{1.4}In_{0.6}$ under the magnetic field cycles [41].

To summarize, we have shown the improved crystallographic compatibility and reversible magnetocaloric using different measurement protocols in 10% Pt substituted $Ni_2Mn_{1.4}In_{0.6}$ magnetic shape memory Heusler alloy. The 10% Pt in $Ni_2Mn_{1.4}In_{0.6}$ reduces thermal hysteresis from ~ 8 K to ~ 4 K. The origin of the reduced thermal hysteresis is found to be related with the reduced middle eigenvalue λ_2 of the phase transformation matrix U. The calculated middle eigenvalue of the U is very close to 1 (0.9982) suggesting crystallographic compatibility between austenite and martensite phases. Moreover, nearly the same ΔS_{iso} values calculated under three different measurement protocols (isothermal, loop, and isofield protocol) indicate a reversible MCE in $Ni_{1.9}Pt_{0.1}Mn_{1.4}In_{0.6}$. However, a direct adiabatic temperature change measurement (magnetocaloric) under magnetic field cycle will be further useful to put this alloy system forward for magnetic cooling device applications. Our study shows that the energy barrier or the stress of the transition layer between austenite and martensite phases in magnetic shape memory Heusler alloys can be reduced via designing suitable composition, which provides crystallographic compatibility and the invariant habit plane between two crystallographic phases and hence a reversible martensite phase transition and magnetocaloric effect.

*ssingh.mst@iitbhu.ac.in

Acknowledgments-

We thank C.F. for encouragement and L.C. for useful discussion. SS thanks Science and Engineering Research Board of India for financial support through the award of Ramanujan Fellowship (grant no: SB/S2IRJN-015/2017), Early Career Research Award (grant no:

ECR/2017/003186) and UGC-DAE CSR, Indore for financial support through “CRS” Scheme. KKD thanks DST for providing fellowship through DST-INSPIRE scheme.

References

- [1] Yu B F, Gao Q, Zhang B, Meng X Z and Chen Z 2003 Review on research of room temperature magnetic refrigeration *International Journal of Refrigeration* **26** 622-36
- [2] Gschneidner Jr K A, Pecharsky V and Tsokol A 2005 Recent developments in magnetocaloric materials *Reports on progress in physics* **68** 1479
- [3] Brown G V 1976 Magnetic heat pumping near room temperature *Journal of Applied Physics* **47** 3673-80
- [4] Nikitin S A, Myalikgulyev G, Tishin A, Annaorazov M, Asatryan K A and Tyurin A L 1990 The magnetocaloric effect in Fe₄₉Rh₅₁ compound *Physics Letters A* **148** 363–6
- [5] Krenke T, Duman E, Acet M, Wassermann E F, Moya X, Mañosa L and Planes A 2005 Inverse magnetocaloric effect in ferromagnetic Ni–Mn–Sn alloys *Nature Materials* **4** 450-4
- [6] Krenke T, Duman E, Acet M, Wassermann E F, Moya X, Mañosa L, Planes A, Suard E and Ouladdiaf B 2007 Magnetic superelasticity and inverse magnetocaloric effect in Ni–Mn–In *Physical Review B* **75** 104414
- [7] Singh S, D'Souza S W, Nayak J, Caron L, Suard E, Chadov S and Felser C 2016 Effect of platinum substitution on the structural and magnetic properties of Ni₂MnGa ferromagnetic shape memory alloy *Physical Review B* **93** 134102
- [8] Pecharsky V K and Gschneidner J K A 1997 Giant Magnetocaloric Effect in Gd₅Si₂Ge₂ *Physical Review Letters* **78** 4494-7
- [9] Hu F-x, Shen B-g, Sun J-r and Wu G-h 2001 Large magnetic entropy change in a Heusler alloy Ni_{52.6}Mn_{23.1}Ga_{24.3} single crystal *Physical Review B* **64** 132412
- [10] Fujita A, Fujieda S, Hasegawa Y and Fukamichi K 2003 Itinerant-electron metamagnetic transition and large magnetocaloric effects in La(FexSi_{1-x})₁₃ compounds and their hydrides *Physical Review B* **67**
- [11] Tegus O, Brück E, Buschow K H J and de Boer F R 2002 Transition-metal-based magnetic refrigerants for room-temperature applications *Nature* **415** 150
- [12] Hu F-x, Shen B-g and Sun J-r 2000 Magnetic entropy change in Ni_{51.5}Mn_{22.7}Ga_{25.8} alloy *Applied Physics Letters* **76** 3460-2
- [13] Du J, Zheng Q, Ren W, Feng W, Liu X and Zhang Z 2007 Magnetocaloric effect and magnetic-field-induced shape recovery effect at room temperature in ferromagnetic Heusler alloy Ni–Mn–Sb *Journal of Physics D: Applied Physics* **40** 5523
- [14] Han Z D, Wang D H, Zhang C L, Tang S L, Gu B X and Du Y W 2006 Large magnetic entropy changes in the Ni_{45.4}Mn_{41.5}In_{13.1} ferromagnetic shape memory alloy *Applied Physics Letters* **89** 182507
- [15] Antoni P, Lluís M and Mehmet A 2009 Magnetocaloric effect and its relation to shape-memory properties in ferromagnetic Heusler alloys *Journal of Physics: Condensed Matter* **21** 233201
- [16] Pons J, Cesari E, Seguí C, Masdeu F and Santamarta R 2008 Ferromagnetic shape memory alloys: Alternatives to Ni–Mn–Ga *Materials Science and Engineering: A* **481-482** 57-65
- [17] Ghorbani Zavareh M, Salazar Mejía C, Nayak A K, Skourski Y, Wosnitza J, Felser C and Nicklas M 2015 Direct measurements of the magnetocaloric effect in pulsed magnetic fields: The example of the Heusler alloy Ni₅₀Mn₃₅In₁₅ *Applied Physics Letters* **106** 071904
- [18] Zou J-D, Shen B-G, Gao B, Shen J and Sun J-R 2009 The Magnetocaloric Effect of LaFe_{11.6}Si_{1.4}, La_{0.8}Nd_{0.2}Fe_{11.5}Si_{1.5}, and Ni₄₃Mn₄₆Sn₁₁ Compounds in the Vicinity of the First-Order Phase Transition *Advanced Materials* **21** 693-6
- [19] Shamberger P J and Ohuchi F S 2009 Hysteresis of the martensitic phase transition in magnetocaloric-effect Ni–Mn–Sn alloys *Physical Review B* **79** 144407

- [20] Basso V, Sasso C P, Skokov K P, Gutfleisch O and Khovaylo V V 2012 Hysteresis and magnetocaloric effect at the magnetostructural phase transition of Ni-Mn-Ga and Ni-Mn-Co-Sn Heusler alloys *Physical Review B* **85** 014430
- [21] Liu J, Gottschall T, Skokov K P, Moore J D and Gutfleisch O 2012 Giant magnetocaloric effect driven by structural transitions *Nature Materials* **11** 620
- [22] Kihara T, Xu X, Ito W, Kainuma R and Tokunaga M 2014 Direct measurements of inverse magnetocaloric effects in metamagnetic shape-memory alloy NiCoMnIn *Physical Review B* **90** 214409
- [23] Singh S, Caron L, D'Souza S W, Fichtner T, Porcari G, Fabbri S, Shekhar C, Chadov S, Solzi M and Felser C 2016 Large Magnetization and Reversible Magnetocaloric Effect at the Second-Order Magnetic Transition in Heusler Materials *Advanced Materials* **28** 3321-5
- [24] Zhang X, Zhang H, Qian M and Geng L 2018 Enhanced magnetocaloric effect in Ni-Mn-Sn-Co alloys with two successive magnetostructural transformations *Scientific Reports* **8** 8235
- [25] Pasquale M, Sasso C P, Lewis L H, Giudici L, Lograsso T and Schlagel D 2005 Magnetostructural transition and magnetocaloric effect in Ni₅₅Mn₂₀Ga₂₅ single crystals *Physical Review B* **72** 094435
- [26] Ghahremani M, Aslani A, Hosseinnia M, Bennett L H and Torre E D 2018 Direct and indirect measurement of the magnetocaloric effect in bulk and nanostructured Ni-Mn-In Heusler alloy *AIP Advances* **8** 056426
- [27] Khovaylo V V, Skokov K P, Gutfleisch O, Miki H, Kainuma R and Kanomata T 2010 Reversibility and irreversibility of magnetocaloric effect in a metamagnetic shape memory alloy under cyclic action of a magnetic field *Applied Physics Letters* **97** 052503
- [28] Sokolovskiy V, Buchelnikov V, Skokov K, Gutfleisch O, Karpenkov D, Koshkid'ko Y, Miki H, Dubenko I, Ali N, Stadler S and Khovaylo V 2013 Magnetocaloric and magnetic properties of Ni₂Mn_{1-x}Cu_xGa Heusler alloys: An insight from the direct measurements and ab initio and Monte Carlo calculations *Journal of Applied Physics* **114** 183913
- [29] Tocado L, Palacios E and Burriel R 2006 Adiabatic measurement of the giant magnetocaloric effect in MnAs *Journal of Thermal Analysis and Calorimetry* **84** 213-7
- [30] Sepehri-Amin H, Taubel A, Ohkubo T, Skokov K P, Gutfleisch O and Hono K 2018 Microstructural origin of hysteresis in Ni-Mn-In based magnetocaloric compounds *Acta Materialia* **147** 342-9
- [31] Ortín J and Delaey L 2002 Hysteresis in shape-memory alloys *International Journal of Non-Linear Mechanics* **37** 1275-81
- [32] Li K, Li Y, Yu K, Liu C, Gibson D, Leyland A, Matthews A and Fu Y Q 2016 Crystal size induced reduction in thermal hysteresis of Ni-Ti-Nb shape memory thin films *Applied Physics Letters* **108** 171907
- [33] Stern-Taulats E, Castillo-Villa P O, Mañosa L, Frontera C, Pramanick S, Majumdar S and Planes A 2014 Magnetocaloric effect in the low hysteresis Ni-Mn-In metamagnetic shape-memory Heusler alloy *Journal of Applied Physics* **115** 173907
- [34] Singh S, Dutta B, D'Souza S W, Zavareh M, Devi P, Gibbs A, Hickel T, Chadov S, Felser C and Pandey D 2017 Robust Bain distortion in the premartensite phase of a platinum-substituted Ni₂MnGa magnetic shape memory alloy *Nature communications* **8** 1006
- [35] Sharma V, Chattopadhyay M, Kumar R, Ganguli T, Tiwari P and Roy S 2007 Magnetocaloric effect in Heusler alloys Ni₅₀Mn₃₄In₁₆ and Ni₅₀Mn₃₄Sn₁₆ *Journal of Physics: Condensed Matter* **19** 496207
- [36] Mañosa L, González-Alonso D, Planes A, Bonnot E, Barrio M, Tamarit J-L, Aksoy S and Acet M 2010 Giant solid-state barocaloric effect in the Ni-Mn-In magnetic shape-memory alloy *Nature Materials* **9** 478
- [37] Titov I, Acet M, Farle M, González-Alonso D, Mañosa L, Planes A and Krenke T 2012 Hysteresis effects in the inverse magnetocaloric effect in martensitic Ni-Mn-In and Ni-Mn-Sn *Journal of Applied Physics* **112** 073914
- [38] Devi P, Singh S, Dutta B, Manna K, D'Souza S, Ikeda Y, Suard E, Petricek V, Simon P and Werner P 2018 Adaptive modulation in the Ni₂Mn_{1.4}In_{0.6} magnetic shape-memory Heusler alloy *Physical Review B* **97** 224102
- [39] Srivastava V, Song Y, Bhatti K and James R D 2011 The direct conversion of heat to electricity using multiferroic alloys *Advanced Energy Materials* **1** 97-104
- [40] Devi P, Mejía C S, Zavareh M G, Dubey K K, Kushwaha P, Skourski Y, Felser C, Nicklas M and Singh S 2019 Improved magnetostructural and magnetocaloric reversibility in magnetic Ni-Mn-In shape-memory Heusler alloy by optimizing the geometric compatibility condition *Physical Review Materials* **3** 062401

- [41] Devi P, Ghorbani Zavareh M, Mejía C S, Hofmann K, Albert B, Felser C, Nicklas M and Singh S 2018 Reversible adiabatic temperature change in the shape memory Heusler alloy Ni_{2.2}Mn_{0.8}Ga: An effect of structural compatibility *Physical Review Materials* **2** 122401
- [42] Singh S, Rawat R and Barman S R 2011 Existence of modulated structure and negative magnetoresistance in Ga excess Ni-Mn-Ga *Applied Physics Letters* **99** 021902
- [43] Wang W H, Liu Z H, Zhang J, Chen J L, Wu G H, Zhan W S, Chin T S, Wen G H and Zhang X X 2002 Thermoelastic intermartensitic transformation and its internal stress dependency in Ni₅₂Mn₂₄Ga₂₄ single crystals *Physical Review B* **66** 052411
- [44] Singh S, Kushwaha P, Scheibel F, Liermann H-P, Barman S R, Acet M, Felser C and Pandey D 2015 Residual stress induced stabilization of martensite phase and its effect on the magnetostructural transition in Mn-rich Ni-Mn-In/Ga magnetic shape-memory alloys *Physical Review B* **92** 020105
- [45] Ranjan R, Singh S, Boysen H, Trots D, Banik S, Awasthi A M, Mukhopadhyay P K and Barman S R 2009 Competing tetragonal and monoclinic phases in Ni_{2.2}Mn_{0.8}Ga *Journal of Applied Physics* **106** 033510
- [46] Caron L, Ou Z Q, Nguyen T T, Cam Thanh D T, Tegus O and Brück E 2009 On the determination of the magnetic entropy change in materials with first-order transitions *Journal of Magnetism and Magnetic Materials* **321** 3559-66
- [47] Luana C, Nguyen Ba D and Laurent R 2017 On entropy change measurements around first order phase transitions in caloric materials *Journal of Physics: Condensed Matter* **29** 075401
- [48] Ghosh A, Sen P and Mandal K 2016 Measurement protocol dependent magnetocaloric properties in a Si-doped Mn-rich Mn-Ni-Sn-Si off-stoichiometric Heusler alloy *Journal of Applied Physics* **119** 183902
- [49] Fabbrici S, Porcari G, Cugini F, Solzi M, Kamarad J, Arnold Z, Cabassi R and Albertini F 2014 Co and In doped Ni-Mn-Ga magnetic shape memory alloys: A thorough structural, magnetic and magnetocaloric study *Entropy* **16** 2204-22
- [50] Ma S, Su Y, Huang Y, Wu Y and Zhong Z 2015 Magnetic and Magnetocaloric Properties in Ferrimagnetic Mn_{2-x}CoxSb (x=0.15 and 0.20) Alloys *IEEE Transactions on Magnetics* **51** 1-6
- [51] Zarnetta R, Takahashi R, Young M L, Savan A, Furuya Y, Thienhaus S, Maaß B, Rahim M, Frenzel J, Brunken H, Chu Y S, Srivastava V, James R D, Takeuchi I, Eggeler G and Ludwig A 2010 Identification of Quaternary Shape Memory Alloys with Near-Zero Thermal Hysteresis and Unprecedented Functional Stability *Advanced Functional Materials* **20** 1917-23
- [52] Cui J, Chu Y S, Famodu O O, Furuya Y, Hatrick-Simpers J, James R D, Ludwig A, Thienhaus S, Wuttig M, Zhang Z and Takeuchi I 2006 Combinatorial search of thermoelastic shape-memory alloys with extremely small hysteresis width *Nat Mater* **5** 286-90
- [53] Song Y, Chen X, Dabade V, Shield T W and James R D 2013 Enhanced reversibility and unusual microstructure of a phase-transforming material *Nature* **502** 85-8
- [54] Jian L and James R D 1997 Prediction of microstructure in monoclinic LaNbO₄ by energy minimization *Acta Materialia* **45** 4271-81
- [55] Zhang Z, James R D and Müller S 2009 Energy barriers and hysteresis in martensitic phase transformations *Acta Materialia* **57** 4332-52
- [56] Srivastava V, Chen X and James R D 2010 Hysteresis and unusual magnetic properties in the singular Heusler alloy Ni₄₅Co₅Mn₄₀Sn₁₀ *Applied Physics Letters* **97** 014101
- [57] Bhattacharya K and James R D 2005 The Material Is the Machine *Science* **307** 53-4
- [58] K. Bhattacharya 2003 Microstructure of Martensite: Why It Forms and How It Gives Rise to the Shape-Memory Effect *Oxford Univ. Press*
- [59] Le Bail A, Duroy H and Fourquet J L 1988 Ab-initio structure determination of LiSbWO₆ by X-ray powder diffraction *Materials Research Bulletin* **23** 447-52
- [60] Singh S, Maniraj M, D'Souza S W, Ranjan R and Barman S R 2010 Structural transformations in Mn₂NiGa due to residual stress *Applied Physics Letters* **96** 081904
- [61] Ranjan R, Banik S, Barman S R, Kumar U, Mukhopadhyay P K and Pandey D 2006 Powder x-ray diffraction study of the thermoelastic martensitic transition in Ni₂Mn_{1.05}Ga_{0.95} *Physical Review B* **74** 224443
- [62] Brown P J, Crangle J, Kanomata T, Matsumoto M, Neumann K U, Ouladdiaf B and Ziebeck K R A 2002 The crystal structure and phase transitions of the magnetic shape memory compound Ni₂MnGa *Journal of Physics: Condensed Matter* **14** 10159-71

- [63] Hane K F and Shield T 1999 Microstructure in the cubic to monoclinic transition in titanium–nickel shape memory alloys *Acta materialia* **47** 2603-17
- [64] Pitteri M and Zanzotto G 1998 Generic and non-generic cubic-to-monoclinic transitions and their twins11Dedicated to Prof. I. Müller on his 60th birthday *Acta Materialia* **46** 225-37
- [65] James R D and Hane K F 2000 Martensitic transformations and shape-memory materials *Acta materialia* **48** 197-222
- [66] Pitteri M and Zanzotto G 2002 *Continuum models for phase transitions and twinning in crystals*: Chapman and Hall/CRC)
- [67] Zhao D, Liu J, Chen X, Sun W, Li Y, Zhang M, Shao Y, Zhang H and Yan A 2017 Giant caloric effect of low-hysteresis metamagnetic shape memory alloys with exceptional cyclic functionality *Acta Materialia* **133** 217-23
- [68] Liu J, Gong Y, You Y, You X, Huang B, Miao X, Xu G, Xu F and Brück E 2019 Giant reversible magnetocaloric effect in MnNiGe-based materials: Minimizing thermal hysteresis via crystallographic compatibility modulation *Acta Materialia* **174** 450-8
- [69] Salazar-Mejía C, Kumar V, Felser C, Skourski Y, Wosnitza J and Nayak A K 2019 Measurement-Protocol Dependence of the Magnetocaloric Effect in NiCoMnSb Heusler Alloys *Physical Review Applied* **11** 054006
- [70] Ghosh A, Rawat R, Bhattacharyya A, Mandal G, Nigam A and Nair S 2019 Measurement independent magnetocaloric effect in Mn-rich Mn-Fe-Ni-Sn (Sb/In) Heusler alloys *Journal of Magnetism and Magnetic Materials* **476** 92-99
- [71] Khovaylo V V, Skokov K P, Gutfleisch O, Miki H, Takagi T, Kanomata T, Koledov V V, Shavrov V G, Wang G, Palacios E, Bartolomé J and Burriel R 2010 Peculiarities of the magnetocaloric properties in Ni-Mn-Sn ferromagnetic shape memory alloys *Physical Review B* **81** 214406
- [72] Gottschall T, Skokov K P, Burriel R and Gutfleisch O 2016 On the S(T) diagram of magnetocaloric materials with first-order transition: Kinetic and cyclic effects of Heusler alloys *Acta Materialia* **107** 1-8
- [73] Neves Bez H, Yibole H, Pathak A, Mudryk Y and Pecharsky V K 2018 Best practices in evaluation of the magnetocaloric effect from bulk magnetization measurements *Journal of Magnetism and Magnetic Materials* **458** 301-9
- [74] Chen J-H, Us Saleheen A, Adams P W, Young D P, Ali N and Stadler S 2018 On entropy determination from magnetic and calorimetric experiments in conventional giant magnetocaloric materials *Journal of Applied Physics* **123** 145101
- [75] Qu Y H, Cong D Y, Sun X M, Nie Z H, Gui W Y, Li R G, Ren Y and Wang Y D 2017 Giant and reversible room-temperature magnetocaloric effect in Ti-doped Ni-Co-Mn-Sn magnetic shape memory alloys *Acta Materialia* **134** 236-48
- [76] Dincer I, Yüzüak E and Elerman Y 2010 Influence of irreversibility on inverse magnetocaloric and magnetoresistance properties of the (Ni,Cu)₅₀Mn₃₆Sn₁₄ alloys *Journal of Alloys and Compounds* **506** 508-12

Figures

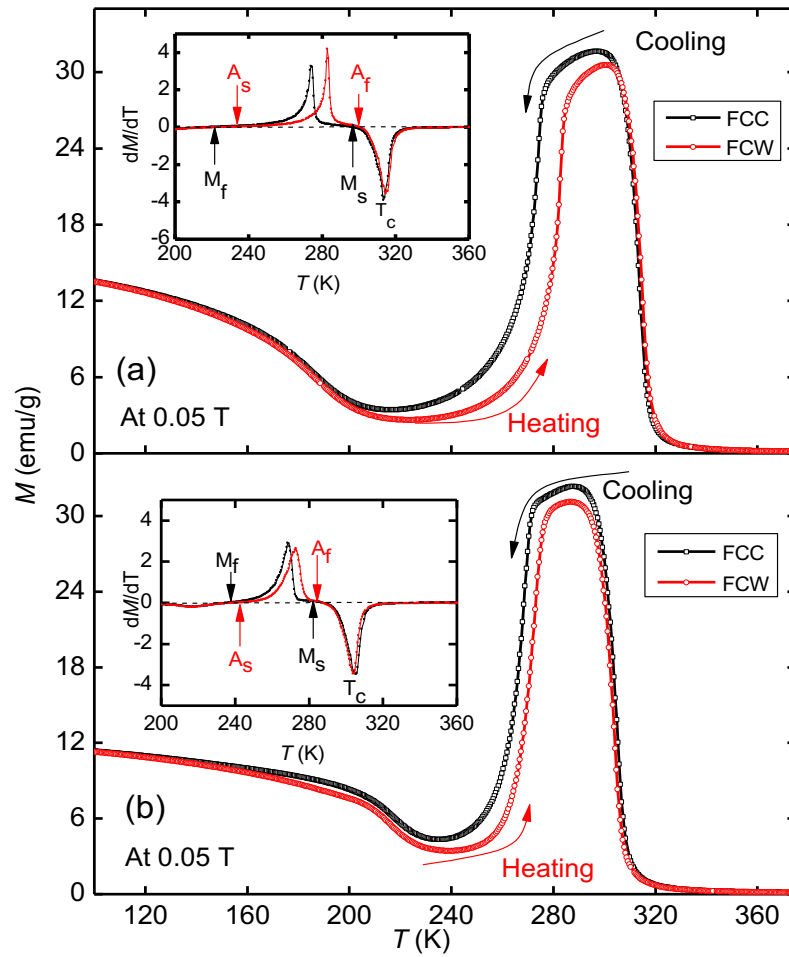


Figure 1. Temperature dependent magnetization curve of (a) $\text{Ni}_2\text{Mn}_{1.4}\text{In}_{0.6}$ and (b) $\text{Ni}_{1.9}\text{Pt}_{0.1}\text{Mn}_{1.4}\text{In}_{0.6}$ at $H=0.05$ T. Insets show differential (dM/dT) curves for better presentation of transition and hysteresis.

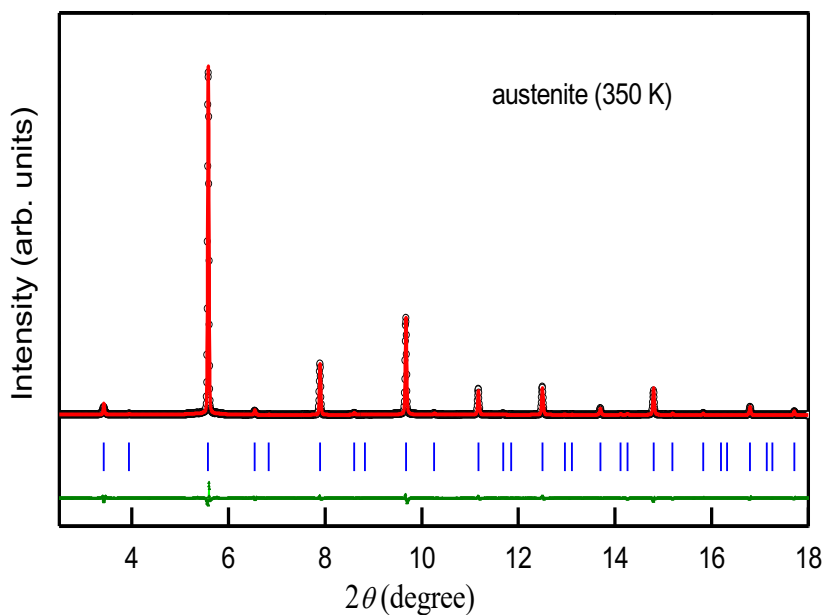


Figure 2. Le Bail refinement of SXRPD data of $\text{Ni}_{1.9}\text{Pt}_{0.1}\text{Mn}_{1.4}\text{In}_{0.6}$ in austenite phase (350 K). The experimental peak profile, calculated peak profile and the difference are shown by black circle, red and green solid lines, respectively. The blue lines represent the Bragg's peak positions.

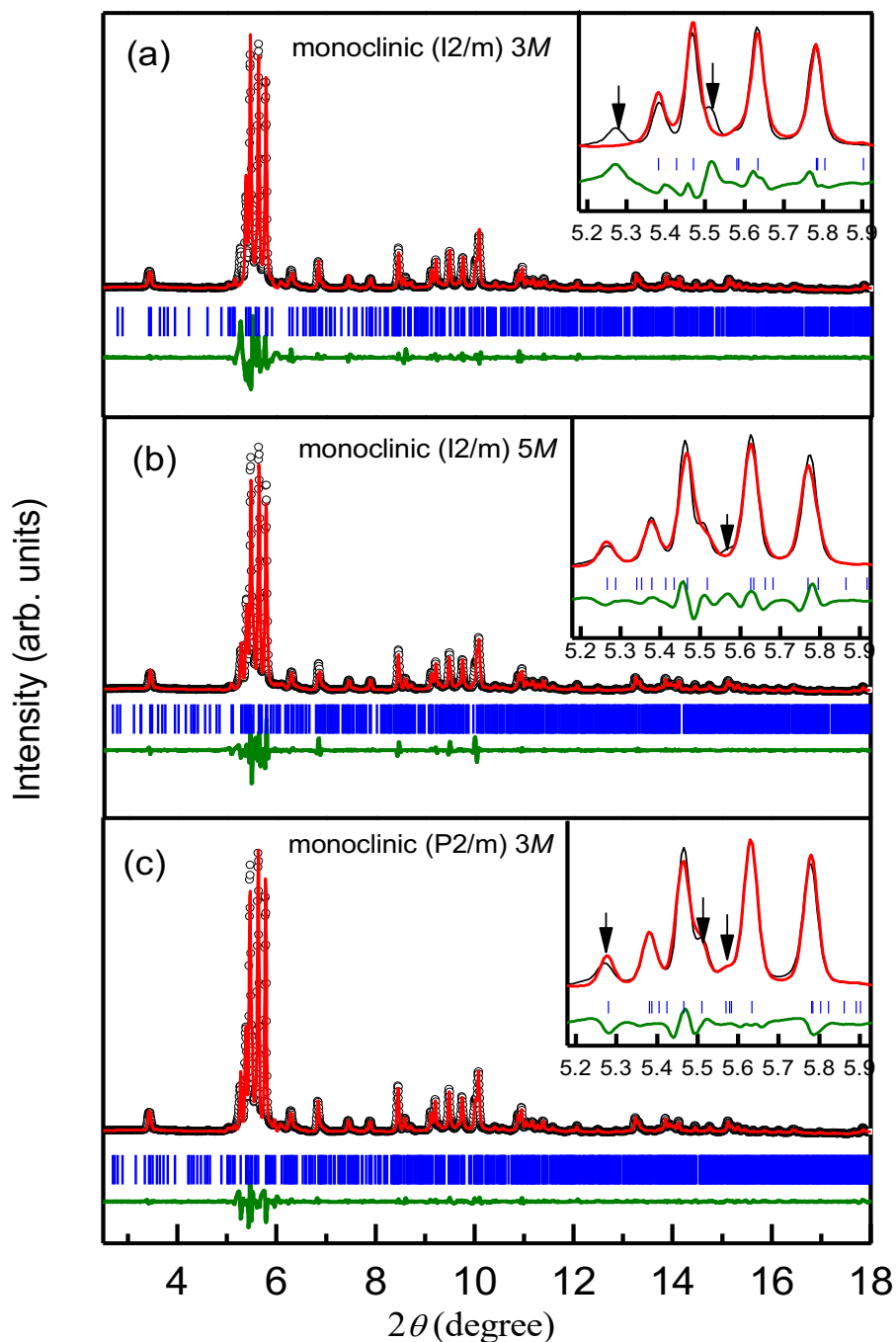


Figure 3. Le Bail refinements of SXRPD data of $\text{Ni}_{1.9}\text{Pt}_{0.1}\text{Mn}_{1.4}\text{In}_{0.6}$ in the martensite phase at 110 K using (a) Monoclinic $3M$ modulated structure (space group: $I2/m$) (b) Monoclinic $5M$ modulated structure (space group: $I2/m$) (c) Monoclinic $3M$ modulated structure (space group: $P2/m$). The experimental peak profile, calculated peak profile and difference are shown by black circle, red and green solid line, respectively. The blue lines represent the Bragg's peak positions. In the insets of (a) and (b), arrows indicate the unindexed peak. In the inset of (c), arrows show the indexed peak which were unindexed in the inset of (a) and (b).

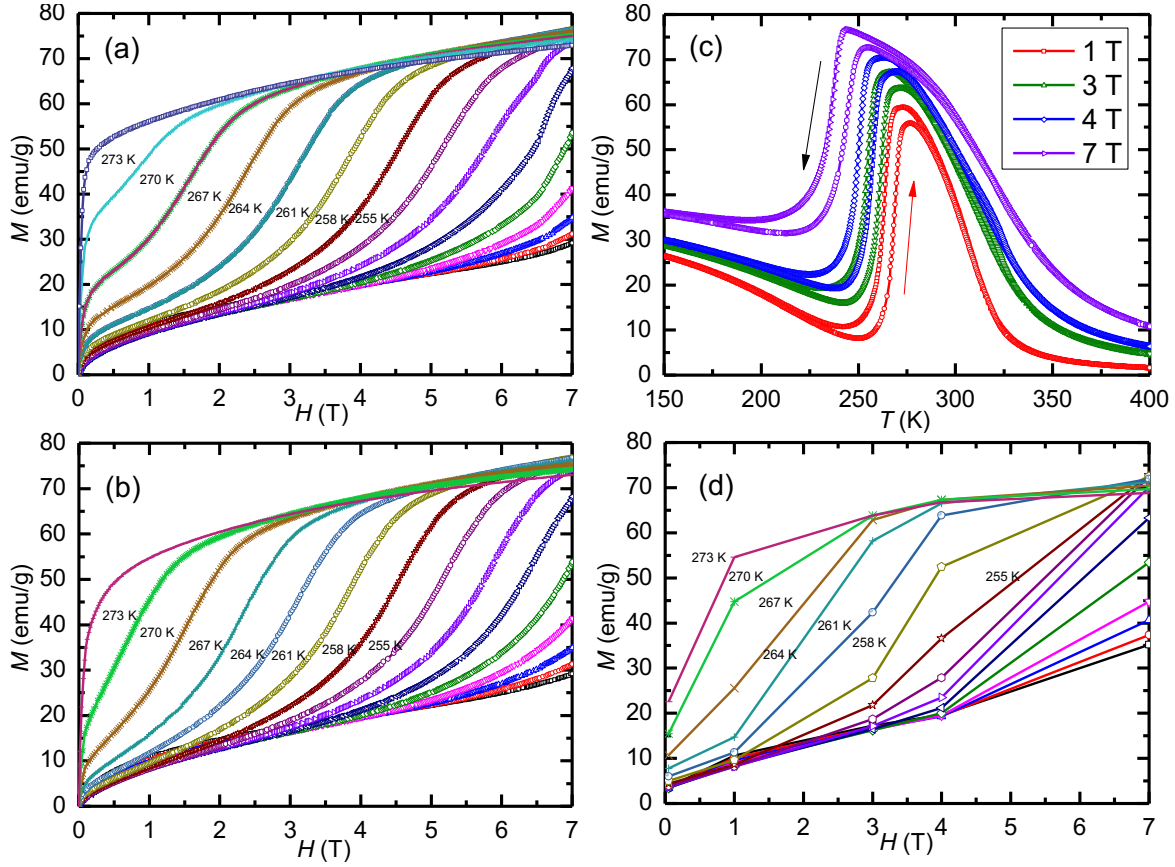


Figure 4. Magnetization measurement results for the $\text{Ni}_{1.9}\text{Pt}_{0.1}\text{Mn}_{1.4}\text{In}_{0.6}$ (a) magnetic isotherms obtained from isothermal measurement protocol. (b) magnetic isotherms obtained from the loop measurement protocol. (c) isofield ($M(T)$) curves of $\text{Ni}_{1.9}\text{Pt}_{0.1}\text{Mn}_{1.4}\text{In}_{0.6}$ at different field values. (d) magnetic isotherms extracted from isofield curves shown in (c).

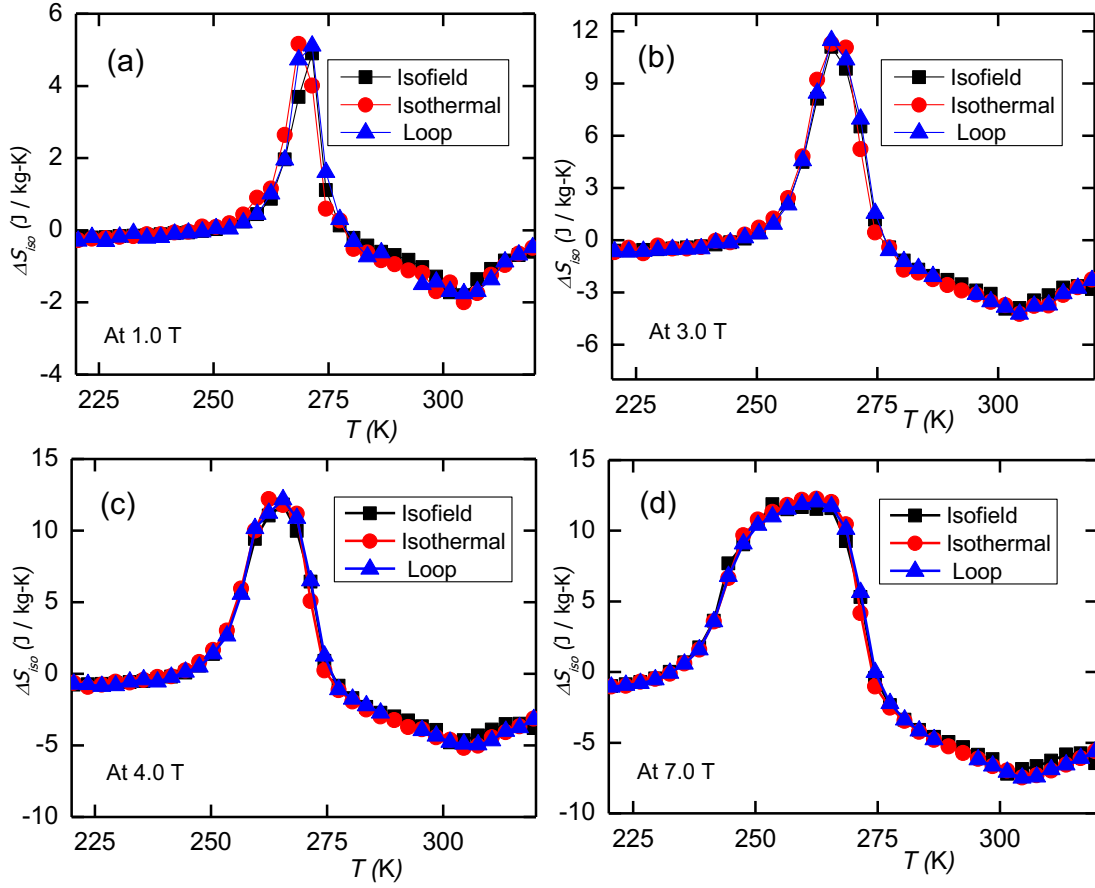


Figure 5. Comparison of isothermal entropy change ΔS_{iso} as a function of temperature for the isofield, isothermal, and loop measurement protocols for $\text{Ni}_{1.9}\text{Pt}_{0.1}\text{Mn}_{1.4}\text{In}_{0.6}$ at different applied field values (a) 1 T (b) 3 T (c) 4 T and (d) 7 T.